Atomic emission spectroscopy in high electric fields

J. E. Bailey, A. B. Filuk, A. L. Carlson, D. J. Johnson, P. Lake, E. J. McGuire, T. A. Mehlhorn, T. D. Pointon, T. J. Renk, W. A. Stygar, Y. Maron, and E. Stambulchik

Citation: AIP Conference Proceedings **381**, 245 (1996); doi: 10.1063/1.51317
View online: http://dx.doi.org/10.1063/1.51317
View Table of Contents:
http://scitation.aip.org/content/aip/proceeding/aipcp/381?ver=pdfcov
Published by the AIP Publishing

Atomic Emission Spectroscopy in High Electric Fields

J.E. Bailey, A.B. Filuk, A.L. Carlson, D.J. Johnson, P. Lake, E.J. McGuire, T.A. Mehlhorn, T.D.Pointon, T.J. Renk, and W.A. Stygar

Sandia National Laboratories, Albuquerque, N.M., 87185

and

Y. Maron and E. Stambulchik

Weizmann Institute of Science, Rehovot, Israel, 76100

ABSTRACT

Pulsed-power driven ion diodes generating quasi-static, ~10 MV/cm, 1-cm scale-length electric fields are used to accelerate lithium ion beams for inertial confinement fusion applications. Atomic emission spectroscopy measurements contribute to understanding the acceleration gap physics, in particular by combining time- and space-resolved measurements of the electric field with the Poisson equation to determine the charged particle distributions. This unique high-field configuration also offers the possibility to advance basic atomic physics, for example by testing calculations of the Stark-shifted emission pattern, by measuring field ionization rates for tightly-bound low-principal-quantum-number levels, and by measuring transition-probability quenching.

INTRODUCTION

The light-ion beam approach to inertial confinement fusion[1] proposes to achieve the required high energy density by accelerating a lithium ion beam to about 30 MeV using one or two acceleration stages, each driven with a high-power (~100 TW), ~30-nsec-duration pulse. Present experiments at the Particle Beam Fusion Accelerator II (PBFA II) facility routinely generate quasi-static, ~10 MV/cm, ~1 cm scale-length electric fields. This enables experiments studying the physics of the ion beam acceleration gap and these conditions also present a unique opportunity for extending experimental atomic physics into the 10 MV/cm regime. This paper describes our application of atomic spectroscopy to ion diode plasma physics issues, with an emphasis on the atomic physics required to understand the results. In addition, we describe preliminary experiments that illustrate the potential of using data from this device for basic atomic physics.

The primary motivation for atomic emission spectroscopy measurements in ion diodes is the need to understand and control the influence of the acceleration gap charged-particle dynamics on the ion beam brightness. Stark-shift measurements of the electric field distribution can be combined with the Poisson equation to determine key features of the charged-particle behavior[2,3]. Understanding the charged-particle distributions is of fundamental importance as we seek to increase the ion beam brightness because they largely control the enhancement of the ion current above the nominal Child-Langmuir space-charge limit[4,5] and because non-uniformities in the charge density can induce beam microdivergence or steering errors that reduce the focussed intensity[6-9]. Our results[3] show that theory and experiment are in reasonable agreement for the first 5 nsec of the ion beam pulse, but as the ion current grows significant discrepancies arise. The measurements provide evidence for new diode phenomena, including field-limited rather than space-charge-limited ion emission, a region with zero net-charge density near the anode, localized positive net-charge in the middle of the gap, and persistent azimuthal asymmetries. Our recent work has emphasized measurements of the small electric field component perpendicular to the direction of beam acceleration and on measurements of emission from Ba II dopants, both with the aim of improving understanding of ion beam divergence.

A new opportunity for atomic physics measurements is provided by the relatively long duration (tens of nsec) and large volume (~1000 cm^3) of the high-field region. Previous emission spectroscopy Stark effect investigations[2] were limited to electric fields below 1 MV/cm, about an order of magnitude below the fields in the PBFA II acceleration gap. Higher fields are certainly generated in short-pulse laser[10], plasma wakefield acceleration[11], and micro-needle experiments[12]. Also, the effect of high electric fields on hydrogen has been investigated[13] using the motional Stark effect to reach ~3 MV/cm. However, the short duration and/or small volume of the high-field regions has prevented acquisition of atomic spectra from these experiments. The conditions in present PBFA II experiments thus enable studies of the high-field Stark effect that were previously impossible. Comparison of independent calculations and results from different species supply confidence that theoretical predictions of the Stark pattern are accurate to within ± 5-10% at fields up 10 MV/cm. Preliminary results for transitions from the tightly-bound Li I 3d level are consistent with predictions of the electric field ionization threshold, and provide the first experimental evidence for transition probability quenching of these transitions.

EXPERIMENTAL METHODS

The experiments described in this paper were performed using a cylindrically-symmetric applied-magnetic-field ion diode[14-16]. PBFA II supplies a 20 TW,

~20 nsec, 10 MV power pulse through conical magnetically-insulated transmission lines connected to the top and bottom of the diode. The ion beam is accelerated radially inward from the inner surface of a cylindrical anode toward a target placed on the axis. An approximately 3 T magnetic field, applied parallel to the anode, insulates the anode-cathode (AK) gap against electron losses.

The visible spectroscopy diagnostic system[17] collects light from approximately-cylindrical 2-mm-diameter lines of sight aligned parallel to the anode. Multiple lines of sight are used to obtain radial and azimuthal spatial resolution, where the radially-resolved measurements provide a profile across the AK gap and the azimuthal measurements determine the degree of cylindrical uniformity. One configuration determines the global uniformity using lines of sight at opposing azimuths of the 15-cm-radius diode, while a second configuration with 2-10 mm azimuthal spacing measures the uniformity over a small azimuthal sector. The light is transported in fiber optics to remote streaked spectrographs for recording with ~ 1 nsec time resolution. A multiplexing technique enables time-resolved spectra with ~ 50 Å range and 1.5 Å resolution to be recorded simultaneously from 8 different spatial locations on a single spectrograph. Data from 18 locations were obtained in each experiment. The relative spacing of the lines of sight is accurate to $\pm$ 0.2 mm and the absolute accuracy of the line-of-sight bundle relative to the anode surface is $\pm$ 0.5 mm.The timing between spectra is accurate to $\pm$0.4 nsec and the timing accuracy relative to the electrically-recorded diode diagnostics is $\pm$ 2 nsec.

LI I ATOMIC PHYSICS IN HIGH ELECTRIC FIELDS

Most measurements to date have relied on Stark-shifted 2s-2p and 2p-3d emission from lithium neutral atoms. Lithium atoms are launched into the gap when a small fraction of the lithium ions charge exchange in a thin, dense, desorbed contaminant layer near the anode. The charge-exchange origin of the Li neutrals impacts the electric field measurements because the Li neutral atoms acquire a high velocity transverse to the beam acceleration direction, due to the ion beam source divergence. This high transverse velocity results in large Doppler broadening (typically 10-15 Å) that prevents resolution of the individual Stark/Zeeman line components. In addition, measurements on the cathode side of the gap are not possible until neutrals arrive there, typically ~10-15 nsec into the pulse. Nevertheless, the Li I charge-exchange neutral atom emission is convenient, it provides good accuracy without disturbing the normal diode operation, and measurements with neutral atoms provide brighter visible light emission intensities than ion emission measurements. We typically analyze 15-20 lineouts from each spectrum, averaging over 4 nsec intervals to improve the signal-to-noise ratio. A

single Gaussian is fit to each spectral line, with a wavelength uncertainty determined using the fluctuation levels of the entire spectrum[18]. The shift is measured relative to the zero-field wavelength established using emission recorded after the power pulse (when the electric field is zero). The procedure determines the Stark shifts with a typical uncertainty ± 0.2 - 0.4 Å, compared to ~6 Å maximum shifts for the 2s-2p and 20-200 Å maximum shifts for the 2p-3d Li I transitions.

The spectral data provides the Stark shift as a function of time and space. The interpretation of this data requires calculations of the Stark / Zeeman line emission pattern as a function of E and B, for values of E that are higher than any previous terrestrial Stark-shift measurement. Independent calculations were performed at Sandia[19] and at the Weizmann Institute[20] in order to improve confidence in the results. Both calculations use direct diagonalization of the Hamiltonian without invoking a perturbation approach. The Zeeman and Stark effects are treated self-consistently and the effects of high-lying levels are included. The Weizmann Institute calculations also include level shifts due to interaction with continuum states. The calculations agree to ~1% with available published data[21,22] that extend up to ~ 0.4 MV/cm. A comparison of the two calculations for the Li I 2s-2p transition using B = 6 T and E = 0-11 MV/cm is shown in Figure 1, where the centroid of the emission pattern is averaged over all observation directions (in actual data analysis we take the directions of the electric and magnetic fields and the line of sight into account). Note that the shift is to the blue, so that larger shifts correspond to shorter wavelengths. The impact of the magnetic field strength on the interpretation of the experiments reported here is negligible because the high electric field dominates the centroid shift and the large Doppler broadening prevents observation of the individual line components. A shift assuming a quadratic dependence on E is also shown in Figure 1. The shift in both calculations is approximately quadratic in E for fields up to about 5 MV/cm, but at higher fields the calculated shifts deviate from the quadratic curve. The quadratic curve was used in the analysis presented below, since it lies between the two detailed calculations and the quadratic approximation is easy to use. At any given shift the fields determined from the two calculations agree to better than ± 5% for fields up to 10 MV/cm. This uncertainty is not included in the error bars presented below. The differences between the calculations at fields above 10 MV/cm are currently under investigation.

A streaked spectrum and a characteristic lineout from a PBFA II experiment are shown in Figure 2. In this experiment we first observe shifted Li I 2s-2p emission at ~56 nsec, simultaneous with the onset of ion current. The Li I 2p-3d emission is not observed until ~78 nsec and when it first appears it is split into red- and blue-shifted components. Interpretation of these data requires an understanding of the various population and de-population rates, as well as accurate calculations of the Stark/Zeeman patterns. The 3d level is initially populated by the same charge-

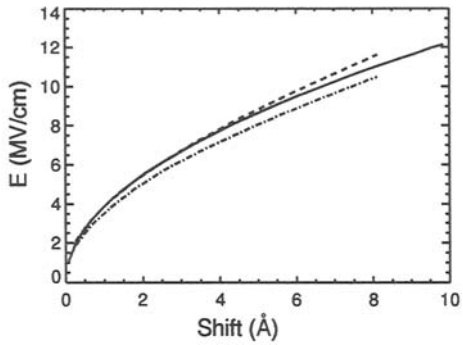

FIGURE 1. Electric field as a function of the Stark / Zeeman emission pattern centroid wavelength shift for the Li I 2s-2p transition at B = 6 T. The dashed curve is from Stambulchik and Maron[20] and the dot-dash curve is from McGuire[19]. The solid curve represents the quadratic relationship, shift (Å) ~ E(MV/cm)^2/15, illustrating the departure of the shift from the quadratic approximation at fields above about 5 MV/cm.

exchange events that populate the 2p level, as well as by ion impact excitation from the 2p level. The dominant de-excitation mechanisms are expected to be field ionization and radiative decay. Prior measurements of the state-selective charge-exchange cross section[23] indicate significant 3d population should be present early in the power pulse. However, the 2p-3d emission is not observed until near the end of pulse. This is almost certainly because the 3d electrons rapidly field ionize under the 5 - 10 MV/cm field. This is consistent with previous detailed calculations of the field ionization rate[24] and expectations based on semiclassical approximations.

As noted above, the 2p-3d is split into red-shifted and blue-shifted components when it first appears. The red-shifted component arises from the 3d $m_L = 2$ state and the blue-shifted component is a superposition of transitions originating from the 3d $m_L = 0,1$ states (throughout the text m_L refers to the absolute value of the orbital angular momentum quantum number). The $m_L = 2$ transition is red-shifted, and is less strongly perturbed, because the selection rules prohibit the 3p level from perturbing the 3d $m_L = 2$ state.The red-shifted feature appears first. The appearance of the blue-shifted feature is delayed because this component has a lower threshold for field ionization and it is more strongly shifted once it does appear. The larger Stark shift of the $m_L = 0,1$ states and the existence of even small electric field variations along the line of sight tends to smear the blue-shifted transitions into a broad line, making it more difficult to observe above the continuum. The field measured from the red-shifted feature is consistent with the field obtained from the 2s-2p transition (Figure 3; a more complete analysis including the shift of the $m_L = 0,1$ component and extraction of uncertainties from the data is in progress). While this agreement is satisfying, it does not represent a stringent test of the Stark pattern calculations because the uncertainty associated with measuring the field from the

2s-2p transition grows as the field shrinks below about 3 MV/cm. During the time of overlap the typical uncertainties for the fields measured from the 2s-2p and 2p-3d transitions are ± 50% and ± 5%, respectively. Note that the uncertainty for field measurements with the 2s-2p transition is typically much lower in experiments emphasizing the use of this line to measure higher fields (Reference 3).

The measurement of the 2p-3d emission enables observations of changes in the transition probability due to wavefunction mixing by the high electric field. While this effect is expected, we are unaware of previous experimental measurements for such low-principal-quantum-number levels. The spontaneous emission intensity per unit volume per steradian emitted in a spectral line is $P = n_{ij} A_{ij} h\nu_{ij}$, where n_i is the excited state population density, $h\nu_{ij}$ is the transition energy, and A_{ij} is the Einstein coefficient. The spontaneous transition probability A_{ij} from excited state i to final state j is proportional to the square of the dipole matrix element, $A_{ij} \sim \langle i|H|j\rangle^2$, where H is the Hamiltonian. The electric field mixes the wavefunctions and A_{ij} depends on the extent of the mixing and, thus, on the field strength. Measurements of the line component intensities therefore reflect changes

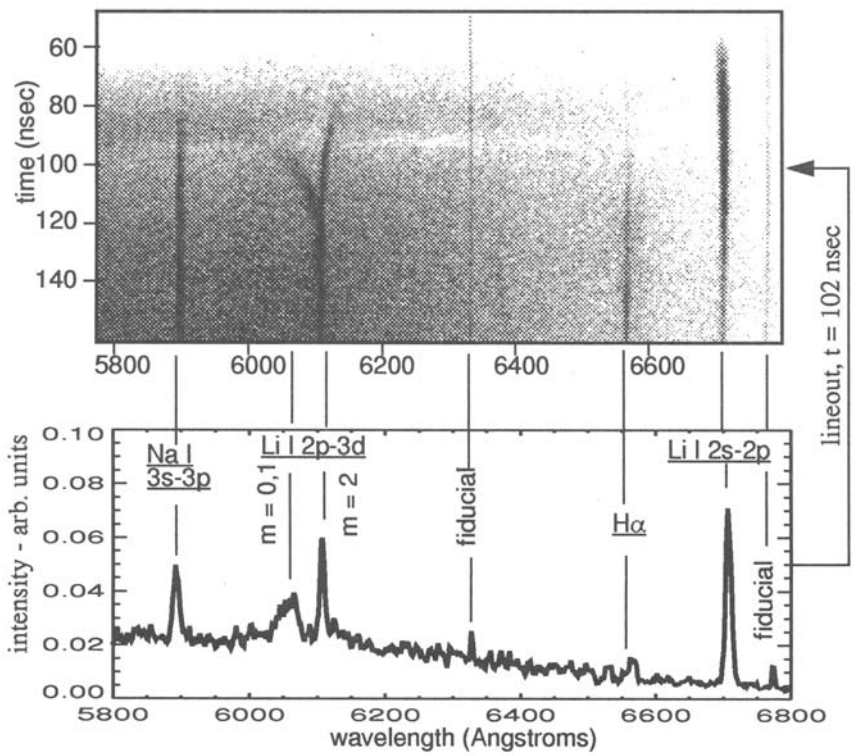

FIGURE 2. Top: Streaked spectrum measured 9 mm from the PBFA II anode surface. Bottom: Lineout averaging over 4 nsec, centered about t = 102 nsec.

in the transition probability caused by the electric field. Calculations of the change in the transition probability performed using the computer code described in Reference 20 show that the transition probability for the m_L =0,1 component decreases by about 30% as the field increases from zero up to 3 MV/cm. The m_L = 2 component changes by only a few percent. The larger change for the m_L = 0,1 component is because these levels mix strongly with the nearby 3p level, while the m_L= 2 does not.

Measurements and calculations of the 3d m_L= 0,1 to 3d m_L = 2 intensity ratio are shown as a function of the electric field in Figure 4. The data and calculations are normalized so that the intensities from the two features are set equal at zero

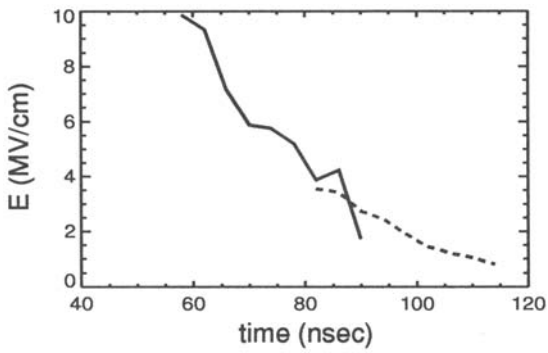

FIGURE 3. Electric field measured from the data shown in Figure 2. The solid curve is the result from Li I 2s-2p and the dashed curve is from Li I 2p - 3d (m_L = 2).

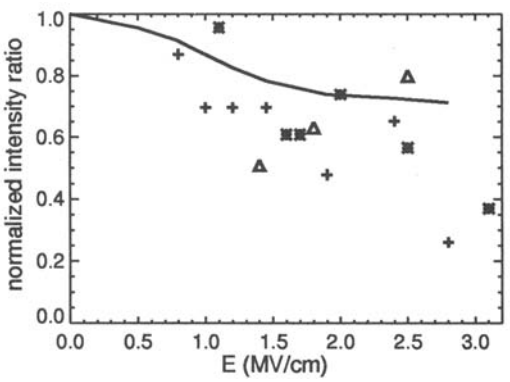

FIGURE 4. Intensity ratio of the Li I 2p-3d components {m_L = 0,1} / {m_L = 2}, normalized to zero electric field. The solid line is a calculation based on Reference 20. The plus, asterix, and triangle symbols are measurements from three separate PBFA II experiments. The experimental uncertainty in the ratio is roughly ± 25%.

electric field. The electric field displayed in this plot is measured from the Stark shift of the $m_L = 2$ (red-shifted) component. The data and calculations agree within the $\pm$ 25% experimental uncertainty for fields up to about 2.5 MV/cm, although the theory systematically predicts a larger ratio. At higher fields the experimental ratio sharply decreases, unlike the theory predictions. This may be because the $m_L = 0$ sublevel is affected by field ionization (see below), an effect not included in the calculations. Note that in this analysis we assume other mechanisms that could affect the line intensity ratio are negligible. Plasma effects on the Einstein coefficient such as those discussed in References 25&26 are unimportant because the charged particle densities are[3] below about 5×10^{13} cm^{-3}. Also, the rates for collisional transfer of population between the $m_L = 2$ and $m_L = 0,1$ 3d levels were estimated and are far too low to affect the results. We therefore assumed that the ratio of the $m_L = 0,1$ to $m_L = 2$ excited state populations was defined by the statistical weights and was independent of the field strength. However, the population mechanism is uncertain, as we discuss below, and the population rate may in fact be sensitive to the field. For example, if the population is produced by ion-impact excitation (the most likely explanation at present) the rate depends on the dipole matrix element squared. Thus, for times short compared to the radiative decay time, the light intensity is expected to decrease quadratically with the dipole matrix element squared. This implies that the line intensity ratio should decrease more with increasing E than in the calculation shown in Figure 4, possibly improving the agreement with the data. The data should be regarded as confirming the expected qualitative trends in the theoretical predictions until a more detailed analysis is complete.

The $m_L = 2$ transition first appears at a field of ~ 3.7-3.9 MV/cm. This is roughly consistent with theoretical predictions that this state field ionizes in less than 10 nsec at E ~ 4.6 MV/cm. The $m_L = 0$ and $m_L = 1$ states are expected to field ionize at fields of 3.1 and 3.6 MV/cm, respectively, also consistent with the fields at which they appear. The transitions probably appear at field values lower than the ionization threshold because the field decreases in time and some additional time is required for the population to build up to an observable value after the field ionization stops depleting the level. However, we cannot rule out inaccuracies in the theoretical field ionization threshold until the population mechanism is better understood. At present, it appears that the earliest 3d emission we observe does not arise from charge-exchange neutral atoms created and excited into the 3d level at the anode. The velocity of the charge exchange neutrals during the early part of the pulse is determined in other experiments using measurements of the time-dependent Li I 2s-2p emission intensity on multiple lines of sight at different distances away from the anode. This velocity is typically ~ 50 cm/μsec, corresponding to a ~15-20 nsec time of flight between the anode and the spectroscopic line of sight located 9 mm away. This implies that if the origin of the Li I 2p-3d emission was charge exchange neutrals, they survived the high fields

existing in the AK gap during the ~15-20 nsec prior to the initial observation of the 2p-3d emission (see Figures 3 & 5). Calculations of the field ionization[24] indicate that this is unlikely. Excitation from the Li I 2p state by Li ion impact excitation is also under investigation (electron impact excitation is small because of the relatively-high electron energies in the diode gap). The elapsed time between the field dropping below ~ 4.7 MV/cm (where fast field ionization is expected) and reaching the 3.7-3.9 MV/cm field (where the transition is observed) is about 3-5 nsec. The key question to evaluate for the ion impact excitation hypothesis is whether this is long enough to produce sufficient 3d m_L=2 population to account for the observed intensity, given the measured ion current density and 2p population density. A similar analysis can be applied to the 3d m_L= 0, 1 states. Resolution of these issues may enable testing of theoretical predictions for the field-ionization rates.

APPLICATIONS TO DIODE PLASMA PHYSICS

A temporal sequence of electric field profiles measured from Stark-shifted Li I 2s-2p emission in a single PBFA II experiment is shown in Figure 5. The AK gap in this experiment was 18 mm. The first measurement at 46 nsec corresponds to the onset of ion current. The diode physics aspects of these results are described in Reference 3. The field measured near the anode surface is 9-10 MV/cm, in contrast to the zero field expected for a space-charge-limited plasma ion source. This result is consistent with a recent theoretical hypothesis[27] that the LiF ion source produces Li ions via electron-assisted field desorption. The almost-flat electric field profile near the anode at peak ion power (62 nsec) implies that there is a ~ 2-3 mm thick, zero-net-charge region near the anode, in contrast to the positive net charge suggested by the simulations described in Reference 7. Note that according to the Poisson equation, the net charge density is proportional to the derivative of the field; hence, a field profile with zero slope implies zero net charge density. About 10 mm from the anode the electric field profile reverses its slope from negative to positive, implying a region with localized positive net charge in the middle of the gap. We emphasize, however, that these results are obtained by assuming uniform conditions along the line of sight. The effect of possible non-uniformities on the conclusions is under investigation. Azimuthal asymmetries between the measurements performed on opposite sides of the diode persist over much of the pulse, indicating that E x B drifting electrons are unable to cancel the asymmetries. These results suggest that improvements are required in both experiments and simulations in order to understand the power-coupling efficiency and divergence.

In the cylindrical barrel-diode geometry the electric field that accelerates the ions toward the target is primarily radial. However, non-radial field components can arise from electromagnetic instabilities and/or non-uniformities in the ion emission, cathode plasma, or virtual cathode electron cloud. These non-radial components deflect the ion beam and add to its divergence as it crosses the AK gap, effectively decreasing the beam power density irradiating the target. A method for measuring the field component in the azimuthal direction, E_ϕ (r,ϕ,t), is illustrated in Figure 6. We measure the magnitude of the electric field vector $|E| = [E_r^2 + E_\phi^2 + E_z^2]^{1/2}$ as a function of time on a rectangular array of spectroscopic lines of sight. Each line of sight is represented by a solid circle in Figure 6. The potential at each azimuth V_A or V_B as a function of radius is obtained by integration of the field, using the approximation that $E \sim E_r$. With this method we obtain the potential for adjacent azimuths as a function of radius and time. The azimuthal component of the electric field E_ϕ is then approximately the potential difference between two azimuths V_{AB}, divided by the azimuthal distance between them δ, using the fact that the line integral of E around the dotted path is zero (estimates for the dB/dt term in this equation indicate that this term is negligible). The challenge in applying this method is that the differences in |E| are of order 10%, requiring that the uncertainty in |E| be less than about 5% in order to arrive at statistically significant values for E_ϕ. The typical uncertainty in our present experiments ranges over $\pm$ 2-6% (at 1σ). This is adequate, but the accuracy of E_ϕ would clearly benefit from reduced uncertainties. Preliminary results for $E_\phi(r,t)$ are shown in Figure 7. The azimuthal field component grows with distance from the anode and it fluctuates on a 2-8 nsec time scale. If confirmed, the measured E_ϕ

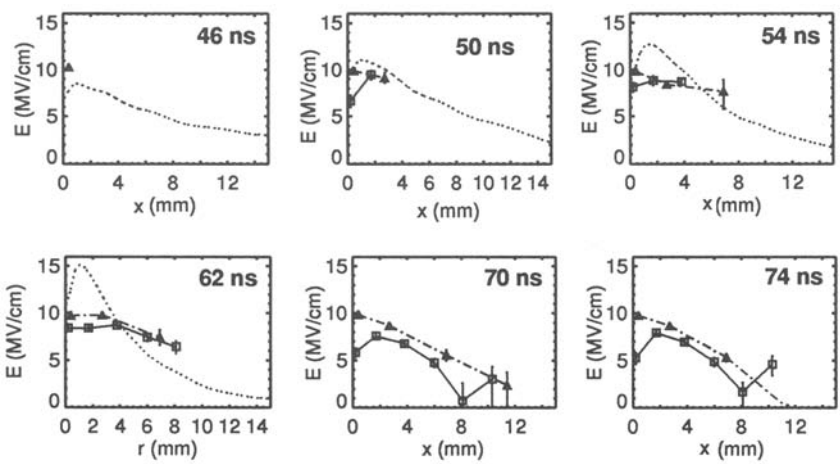

FIGURE 5. Electric field evolution as a function of x, the radial distance away from the anode. The squares and triangles are measurements from a PBFA II experiment at the 180° and 0° azimuths, respectively. The dashed curve is a QUICKSILVER simulation result (Reference 7).

within 5.5 mm of the anode is sufficient to cause ~25 mrad of beam deflection (averaged over the first 1/2-2/3 of the power pulse), comparable to the 25-35 mrad measured at the target on axis. Work is in progress to measure the radial and azimuthal extent of E_ϕ over larger radial and azimuthal distances in order to help identify its origin.

Additional aspects of both atomic physics and diode physics can be explored by adding impurity dopants to the anode. In one such experiment, BaF_2 and LiF were co-evaporated onto the anode in an approximately 1:1 molecular ratio. The primary motivations for adding BaF_2 to the anode were to provide a direct measurement of ion divergence and to enable Zeeman measurements of the magnetic field. Note that the lithium ion beam divergence is very difficult to measure directly because the

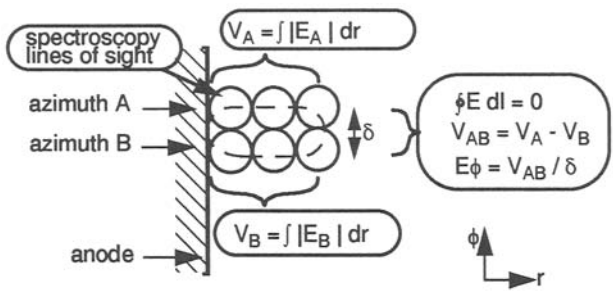

FIGURE 6. Top view of the diode AK gap illustrating the method used to determine the non-radial electric fields from the Stark shift measurements. The circles represent individual spectroscopic lines of sight that are approximately 2 mm in diameter. The dashed curve illustrates the path for the line integral. In actual experiments a larger array of points (up to eighteen total) is used to obtain more complete measurements of the radial and azimuthal dependence.

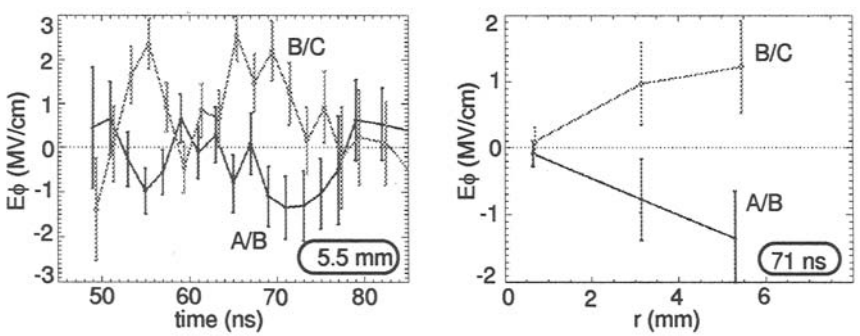

FIGURE 7. Preliminary measurements of the azimuthal component of the electric field obtained using a line of sight arrangement similar to that shown in Figure 6, but with an additional row of lines of sight at a third azimuth. The curves labeled A/B refer to one pair of azimuths and the curves labeled B/C refer to the other pair. Ion current onset in this experiment was at 41 nsec. The time history on the left corresponds to 5.5 mm from the anode surface and the spatial plot on the right corresponds to t = 71 nsec.

lithium ion excited states are not significantly populated. Measurements of Ba II Doppler broadening are straightfoward in comparison to Li II measurements, since the high Ba ion mass makes the Ba ion density relatively high and the easily-excited resonance transition lies in the visible regime. In addition, the Ba II Doppler broadening is expected to be smaller than for the Li I charge-exchange neutrals. This may enable measurements of the magnetic field profile from the Stark / Zeeman pattern.

These diode physics results will be discussed elsewhere. Here, we only point out that simultaneous measurements of the electric field from Ba II and Li I emission provide a useful cross-check of the Stark pattern calculations. A temporal sequence of lineouts measuring the Ba II 6s $^2S_{1/2}$-6p $^2P_{1/2}$ transition are shown in Figure 8. This transition is split into two components, one appearing at the zero-field wavelength and one that is Stark-shifted. The intensity of the unshifted component relative to the shifted feature grows in time. The appearance of a Stark-shifted component verifies that it is indeed possible to observe Ba II emission as the ions are accelerated across the gap. Interpretation of the fact that both shifted and unshifted light are observed simultaneously is in progress, but it appears to be consistent with acceleration of barium ions from both field-threshold-emission regions (as for LiF) and from plasmas. The time-dependent electric field measured from the Li I emission compared to the field determined using the shifted portion of the Ba II emission is shown in Figure 9. The fields agree to within ± 10%, although there is a systematic difference in the field determined form the Ba II 6s $^2S_{1/2}$-6p $^2P_{1/2}$ and 6s $^2S_{1/2}$-6p $^2P_{3/2}$ lines. This is probably due to inaccuracies in the oscillator strengths used in the Stark pattern calculations of Reference 20. Note that better agreement between the Li I and Ba II data cannot be expected, since in the

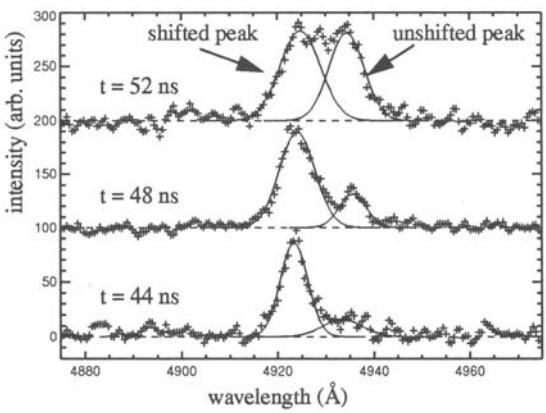

FIGURE 8. A temporal sequence of lineouts for the Ba II 6s $^2S_{1/2}$ - 6p $^2P_{1/2}$ transition, measured adjacent to the PBFA II anode. Each successive time step is displaced by 100 intensity units to facilitate viewing. Gaussian fits to the peaks (solid curves) obtained with the ROBFIT code are superimposed on the data (plus signs). The unshifted (zero field) wavelength is 4934.1 Å.

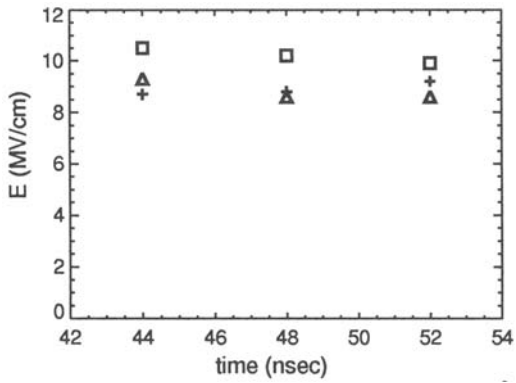

FIGURE 9. Electric field measured from Li I 2s-2p (triangle), Ba II 6s $^2S_{1/2}$-6p $^2P_{1/2}$,(squares), and 6s $^2S_{1/2}$-6p $^2P_{3/2}$ (plus sign) lines. The average deviation is less than 8%.

present experiment the Ba II and Li I emission were collected with lines of sight located at the same radial distance from the anode, but at adjacent azimuths separated by 2 mm. Data described above shows that differences of about 10% in |E| can exist over this azimuthal separation. We plan to perform a more stringent test of these Stark pattern calculations by collecting light in a single line of sight and splitting it into two streaked spectrographs. This should enable a cross-comparison of the Li I and Ba II results to within approximately $\pm$ 5%.

CONCLUSIONS

Measurements of Stark-shifted emission clearly provide new insight into the complex plasma physics in ion diode acceleration gaps. In particular, these measurements enable comparisons of the 3-D electromagnetic simulations that are used to predict diode operation with detailed measurements for the first time. Interpretation of the measurements requires accurate calculations of the line emission patterns under ~ 10 MV/cm electric fields and 3 - 6 T magnetic fields. In addition, the high field routinely produced on PBFA II invites basic atomic physics measurements for low-lying levels that were previously impossible. Measurements of the Li I 2p-3d transitions are consistent with calculations of field ionization thresholds, although stringent tests of the calculations require progress in understanding level population mechanisms. Preliminary measurements of the dependence of the line component intensities on the electric field are also consistent with predictions.

ACKNOWLEDGMENT

We would like to thank the PBFA II operations crew, P.M. Baca, and D.F. Wenger for technical assistance. We are also grateful to S.A. Slutz, T.R. Lockner, M.P. Desjarlais, and T. Nash for many useful discussions and to D.L. Cook, R.J. Leeper, and J.P. Quintenz for continuous support and encouragement. This work was supported by the U.S. Department of Energy under contract No. DE-AC04-94AL85000.

REFERENCES

1. J. P. VanDevender and D.L. Cook, *Science*, **232**, 801 (1986).
2. Y. Maron, M.D. Coleman, D.A. Hammer, and H.S. Peng, *Phys. Rev. Lett.* **57**, 699 (1986), *Phys. Rev. A.* **36**, 2818 (1987).
3. J.E. Bailey et al., *Phys. Rev. Lett.* **74**,1771 (1995).
4. S.A. Slutz, D.B. Seidel, and R.S. Coats, *J. Appl. Phys.* **59**, 11 (1986).
5. M.P. Desjarlais, *Phys. Rev. Lett.* **59**, 2295 (1987).
6. M.P. Desjarlais et.al., *Phys. Rev. Lett.* **67**, 3094 (1991).
7. T.D. Pointon et.al., *Phys. Plasmas* **1**, 429 (1994).
8. S.A. Slutz and W.A. Johnson, *Phys. Fluids* **B4**, 1349 (1992).
9. S.A. Slutz, *Phys. Fluids B* **4**, 2645 (1992).
10. P.H. Bucksbaum, in *Atoms in Strong Fields*, Ed. by C.A. Nicolaides, C.W. Clark, and M.N. Nayfeh, Plenum Press, New York, 1990 (NATO ASI Series B: Physics Vol. 212) p. 381.
11. K. Nakajima et al., *Phys. Rev. Lett.* **74**, 4428 (1995).
12. A.L. Pregenzer et al., *J. Appl. Phys.* **67**, 7556 (1990).
13. T. Bergeman et al., *Phys. Rev. Lett.* 53, 775 (1984).
14. S. Humphries, Jr., *Nucl. Fusion* **20**, 1549 (1980).
15. D.J. Johnson et. al., *J. Appl. Phys.* **53**, 4579 (1982) and *Proc. 7th IEEE Pulsed Power Conf*, Monterey, CA, 1989, ed. by R. White and B.H. Bernstein, p. 944.
16. T.A. Mehlhorn, in *Proc. of 10th Int. Conf. on High Power Particle Beams*, San Diego, CA., NTIS # PB95-144317, p. 53 (1994).
17. J. Bailey, A.L. Carlson, R.L. Morrison, and Y. Maron, *Rev. Sci. Instrum.* **61**, 3075 (1990) and J.E. Bailey, A.L. Carlson, and P. Lake, *Proc. 1994 IEEE Int. Conf. on Plasma Sci.*, Santa Fe, IEEE Cat. # 94CH3465-2, p. 133 (1994).
18. R.L. Coldwell and G.J. Bamford, *The Theory and Operation of Spectral Analysis Using Robfit*, AIP, New York (1991).
19. E.J. McGuire, (to be published) 1995.
20. E. Stambulchik and Y. Maron, Weizmann Institute of Science Report WIS-90/40/Sept.-PH (1994).
21. L.R. Hunter, D. Krause, Jr., D.J. Berkeland, and M.G. Boshier, *Phys. Rev. A* **44**, 6140 (1991).
22. L. Windholz, M. Musso, G. Zerza, and H. Jager, *Phys. Rev. A* **46**, 5812 (1992).
23. R. Odom et al., *Phys. Rev. A* **14**, 965 (1976).
24. S.I. Themelis & C.A. Nicolaides *Phys. Rev. A* (1994)
25. H.R. Griem et al., *Phys. Fluids B* **3**, 2430 (1991).
26. S. Suckewer, *Phys. Fluids B* **3**, 2437 (1991).
27. T.A. Green, Sandia Report SAND95-1794 (available from NTIS, U.S. Dept. of Commerce, 5285 Port Royal Road, Springfield, VA. 22161) (1995), and R.W. Stinnett et.al, *Proc. 9th Int. Conf. on High Power Particle Beams*, Washington DC, NTIS PB92-206168, p. 788 (1992).